

Received January 15, 2019, accepted January 31, 2019, date of publication February 4, 2019, date of current version February 27, 2019.

Digital Object Identifier 10.1109/ACCESS.2019.2897381

# On the Probabilistic Shaping and Geometric Shaping in Optical Communication Systems

ZHEN QU<sup>1</sup>, (Student Member, IEEE), AND IVAN B. DJORDJEVIC<sup>1</sup>, (Senior Member, IEEE)

Department of Electrical and Computer Engineering, The University of Arizona, Tucson, AZ 85721, USA

Corresponding author: Zhen Qu (zhenqu@email.arizona.edu).

This paper was supported in part by the MURI Program, Office of Naval Research (ONR), under Grant N00014-13-1-0627.

**ABSTRACT** We introduce and compare typical shaping schemes suitable for optical communications. The geometrically shaped-quadrature amplitude modulation (GS-QAM) formats are characterized by the non-equidistant spacing of constellation points, transmitted uniformly, and applied to improve system capacity. On the other hand, the well-known constant composition distribution matcher (CCDM) is applied for the generation of probabilistically shaped QAM (PS-QAM) formats. Mutual information (MI) is used as a metric to analyze the performances of regular/GS/PS-MQAM formats. In a linear amplified spontaneous emission noise limited region, it can be proved by the numerical simulation that MI performances of the GS-8/16QAM are always better than regular 8/16QAM and PS-8/16QAM; the largest shaping gains can be separately reached by PS-32QAM and GS-32QAM. We continue with the experimental demonstration on the 16QAM-based transmission system, and find that GS-16QAM generally has the best MI performance. We also find that the modulation-dependent nonlinear noises of the GS-8/16/32QAM are comparable to that of the regular 8/16/32QAM and generally lower than PS-8/16/32QAM. By using the enhanced Gaussian noise model, we observe that the GS-8/16QAM formats have better performances than regular 8/16QAM and PS-8/16QAM over multi-span transmission. Meanwhile, PS-32QAM formats provide superior performance over a relatively long transmission distance.

**INDEX TERMS** Geometric shaping, mutual information, nonlinear distortion, optical fiber communication, probabilistic shaping, quadrature amplitude modulation.

## I. INTRODUCTION

The ever-growing Internet traffic has been pushing forward the development of optical transport networks for decades. As an enabling technology for power-efficient and spectrally efficient communications, coherent detection combined with digital signal processing (DSP) has prevailed throughout various state-of-the-art optical transmission systems [1]–[3]. Advanced modulation formats have been widely applied to improve the spectral efficiency [4], [5]; a series of multiplexing techniques have been explored to boost the aggregate capacity [6], [7]. Called upon the demand of higher data rate, the telecommunication industry has put on the agenda the single-carrier 400G optical transmission. The 16-quadrature amplitude modulation (16QAM) format has been proposed as a potential solution. The 16QAM can relieve the hardware requirement, which offers a cost-efficient solution [8].

Although uniform QAM formats are usually deployed in the modern optical transports for the facility of generation

and detection, there is an asymptotic loss of  $\pi e/6$  ( $\approx 1.53$  dB) towards the Shannon limit [9], as shown in Fig. 1. According to the information theory, such 1.53 dB gap can be closed by the shaping gain if the modulation format yields a Gaussian distribution. It is worthwhile to notice that both coding and shaping are the key technologies to approach the Shannon limit, but they play different roles. Coding attempts to maximize the distance between code vectors; while shaping is performed to minimize the average symbol energy, and result in the larger Euclidean distance among constellation points at the same power level [10]. Since channel coding for optical communications has reached its maturity [11], constellation shaping is becoming the last resort to realize capacity-approaching optical communications.

Shaping gain can be obtained by geometric shaping (GS) or probabilistic shaping (PS) [12]–[15]. Compared to the regular QAM formats, where each constellation point is located on a uniform Cartesian grid and sent with equal probability, GS-QAM allows a non-equidistant constellation distribution. In comparison, the constellation points in a PS-QAM format are sent with different probabilities. Despite the

The associate editor coordinating the review of this manuscript and approving it for publication was San-Liang Lee.

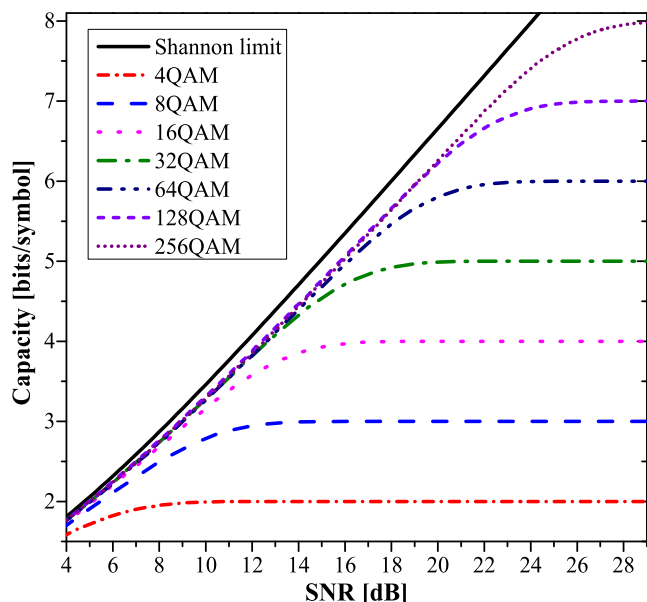


FIGURE 1. Capacity of uniform MQAM formats.

difference between the GS and PS schemes, they both mimic a quantized sampled Gaussian distribution, and are able to closely approach the Shannon limit within finite dimensions. In addition, hybrid GS/PS schemes have also been proposed recently [16]–[18]. Although more complicated, the hybrid GS/PS schemes are able to further improve the capacity.

The optimal GS constellation depends on the optimization criterion and signal-to-noise ratio (SNR). Available optimization criteria include but are not limited to: minimizing average symbol error probability, maximizing mutual information, and minimizing mean-square error of Gaussian source representation. In general, the constellation points with lower amplitude are spaced closer than the outside points. Several GS-QAM formats, like generalized cross constellation, were proposed in earlier work to achieve the shaping gain [12]. In addition, iterative polar modulation [19], generalized mutual information (GMI)-optimized QAM formats [20], and multidimensional constellation with multi-sphere distribution [21], have been proposed recently as practical GS implementations.

In an additive white Gaussian noise (AWGN) channel, PS constellations usually follow a Maxwell-Boltzmann (M-B) distribution, since M-B distribution can perform close to the optimal distribution with optimized parameters [10]. Basically, the constellation points within a lower power layer are transmitted with a higher probability. As a result, the average symbol power can be reduced. The PS-related research started with Gallager's many-to-one mapping scheme [15]. Then more advanced PS schemes were proposed, e.g., trellis shaping [22] and shell mapping [23]. Given that arithmetic coding (AC) can be used to index sequences efficiently, an AC-based constant composition distribution matcher (CCDM) has been proposed [24]. Then CCDM

based probabilistic amplitude shaping (PAS) was proposed in [25]. PS and differential evolution (DE) based GS have been numerically compared in an AWGN channel [26], which considers the integration of constellation shaping and forward error correction (FEC) coding, and uses the appropriate achievable rate expressions accounting for the employed decoding metrics and provides bit-error rate/frame-error rate (BER/FER) analysis.

Although shaping in principle can lead to capacity-approaching modulation formats, both PS and GS face the implementation penalty problems. There are three major drawbacks in GS-QAM based transmission systems: the gap between GMI and MI can only be closed by nonbinary FEC coding, which is quite challenging for hardware implementation, in particular when the order of Galois field is larger than 4; the digital-to-analog converter/analog-to-digital converter (ADC/DAC) used at the transceiver side require higher resolution; the DSP algorithms for signal recovery generally are not compatible with that of the regular QAM formats. On the other hand, CCDM-based PAS-MQAM transmission systems will also encounter several problems: CCDM is challenging for real-time implementation; multiple bit-to-symbol (B2S) mapping and symbol-to-bit (S2B) mapping applied at the transceiver bring on extra complexity; the entropy loss can only be compensated by shaping on higher-order QAM formats; error propagation after the distribution de-matcher has not been properly resolved; the code rate of FEC coding is lower-bounded by  $[\log_2(M) - 2]/\log_2(M)$ ; blind channel equalization is very difficult, and pilot-tones need to be sent to assist the signal recovery [27]. Besides the aforementioned problems, shaped QAM will also induce additional modulation-dependent nonlinear noise in long-haul transmission systems [28], especially when the constellation is strongly shaped.

In this paper, we introduce a Gaussian-like GS-QAM family, and numerically compare the mutual information (MI) performances of regular/PS/GS-8QAM, regular/PS/GS-16QAM, and regular/PS/GS-32QAM, in an AWGN channel. Then we experimentally study various polarization multiplexed (PM) GS/PS/regular-16QAM schemes over a 100-km fiber-optics transmission system. Our experimental results show that GS-16QAM has a larger shaping gain over regular/PS-16QAM in a wide region of optical SNR (OSNR). Finally, the performances of regular/PS/GS-8/16/32QAM formats are evaluated numerically in a multi-span transmission system.

The remainder of this paper is organized as follows. In Section II, we overview the probabilistic amplitude shaping (PAS) scheme, introduce a GS-QAM generation procedure, describe the MI theory, and compare the MI performances for 8/16/32QAM formats. In Section III, we experimentally explore the MI performances of regular/PS/GS-16QAM in a linear regime, dominated by ASE noise. The nonlinear performances of the 8/16/32QAM formats are analyzed in Sec. IV. Section V summarizes our work.

II. SHAPED MODULATION FORMATS

A. PAS AND GS TECHNIQUES

Figures 2 (a) and (b) show the typical PAS-QAM and GS-QAM based transmission systems. The constellation of the square MQAM can be expressed as the Cartesian product of two pulse-amplitude modulation (PAM) constellations, namely,

$$X = \{\pm 1, \pm 3, \dots, \pm(\sqrt{M} - 1)\} \quad (1)$$

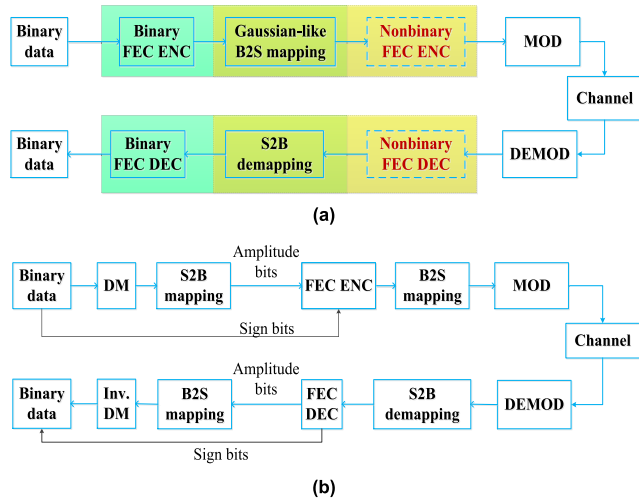


FIGURE 2. Typical transmission systems based on: (a) GS-MQAM and (b) PAS-MQAM.

In a PAS scheme, the PAM constellations in both in-phase and quadrature arms yield the so-called M-B distribution,

$$P_{X_v}(x) = e^{-\nu|x|^2} / \sum_{x' \in X} e^{-\nu|x'|^2} \quad (2)$$

where  $\nu$  is a non-negative scaling factor to determine the entropy. If  $\nu$  is 0, the PAM constellation yields a uniform distribution, and offers the maximum entropy. The CCDDM will map the binary sequences to lexicographically ordered amplitude sequences, followed by S2B mapping and binary FEC coding. In the bit labeling of a PAS-QAM format [25], the sign bits always follow the uniform probability distribution, which can be used for carrying the uniformly distributed parity-check bits. As a result, the PAM constellation still follows M-B distribution after FEC coding and B2S mapping. Notice that the FEC encoding has to be used after the DM to ensure there are no bit errors before the distribution de-matcher.

The GS-MQAM based transmission system is quite similar to that of the regular MQAM. However it remains an open question in which sense the GS-MQAM is optimal. We use the signal constellation design algorithm to obtain the GS-MQAM constellations that aims to minimize the mean-square error of optimum source representation [29], [30]. The iteration steps can be described as follows.

1. Determining the optimal source distribution by the Arimoto-Blahut (A-B) algorithm. In a Gaussian noise limited transmission system, e.g., an amplified spontaneous emission (ASE) noise limited fiber-optic transmission system, the optimal source in

two-dimensional (2D) space is supposed to yield a Gaussian distribution.

2. Choosing the uniformly distributed regular MQAM as the initial constellation.
3. Generating a symbol sequence following the optimal source distribution.
4. Distributing the symbol sequence into M clusters, where the decision is made according to the minimum Euclidean distance from the MQAM constellation points obtained in previous iteration.
5. Finding the average central positions from the symbols labeled by each cluster. The acquired M points located on the central positions are used as the new MQAM constellation points.
6. Iterating over Steps 3 and 5 until convergence.

By independently running the Steps 1-6 hundred times, symmetrical constellation can be finally determined from trials averaged. A symmetrical QAM format is highly desirable for experimental implementation. Notice that the converged constellation is dependent on the variance of the optimal source. By using the proposed procedure, The GS-8/16/32 QAM constellations, as shown in Figs. 3 (a1)- (c1), can only be optimal in a certain SNR region. While, for the simplicity, we apply such GS-8/16/32QAM formats for the whole SNR region. Under the MQAM based transmission system, PS can optimize the performance with the help of flexible entropy; while GS is able to improve the performance by adaptive modulation, with the modulation formats selected from the GS-MQAM family. Considering PAS-64QAM has been able to approach the Shannon limit [27], and GS-64QAM is much more sensitive to the implementation and DSP penalties, we do not suggest applying the GS-64QAM for a realistic transmission system. Therefore, we will not discuss the performance of GS-64QAM in this paper.

B. MI ANALYSIS

MI is directly related to the constellation distribution, and has been used to accurately predict the post-FEC BER performance [31], [32]. In this paper, all the MI results are calculated without the consideration of FEC coding/decoding. In most practical optical communication systems, it is reasonable to assume transmitting a series of independent and identically distributed discrete symbols over a memoryless channel. The discrete channel input, continuous complex output, and the channel transition probability are denoted here by  $X$ ,  $Y$ , and  $P_{Y|X}(y|x)$ , respectively. The mutual information is defined as

$$\begin{aligned} I(X; Y) &= H(X) - H(X|Y) \\ &= - \sum_{x' \in X} P_X(x') \log_2 P_X(x') \\ &\quad + \sum_{x' \in X} P_X(x') \int_C P_{Y|X}(y|x') \\ &\quad \times \log_2 \frac{P_{Y|X}(y|x') P_X(x')}{\sum_{x' \in X} P_{Y|X}(y|x') P_X(x')} dy \quad (3) \end{aligned}$$

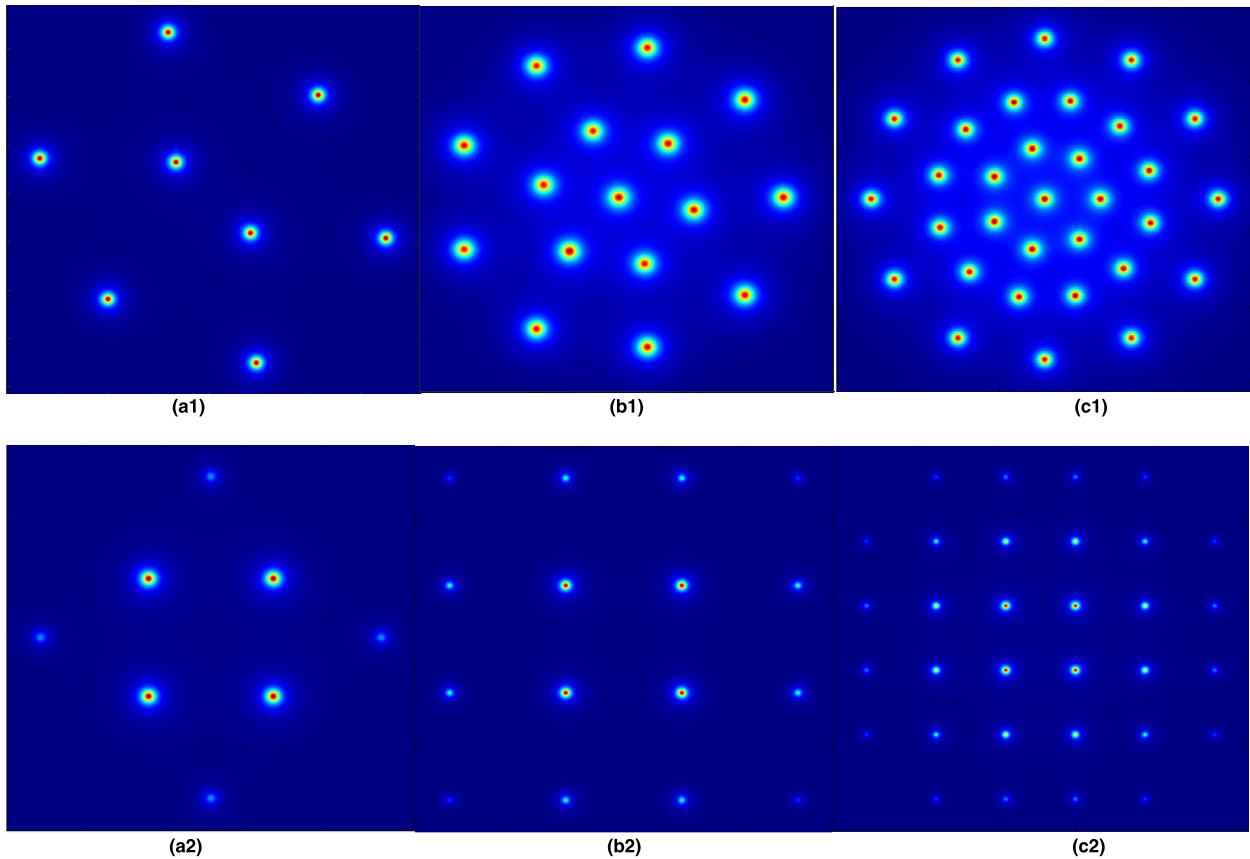


FIGURE 3. The constellation diagrams for (a1) GS-8QAM, (b1) GS-16QAM, (c1) GS-32QAM, and (a2) PS-8QAM, (b2) PS-16QAM, (c2) PS-32QAM.

where  $P_X(x')$  is the probability of the discrete channel input,  $x' \in \chi$ , and  $\chi$  represents the set of MQAM constellation points  $\chi = \{x_1, x_2, \dots, x_M\}$ . However the MI cannot be directly calculated by (3), because there is no closed-form solution for  $P_{Y|X}(y|x)$ . Thanks to the mismatched decoding tool [33], an auxiliary channel with transition probability  $Q_{Y|X}(y|x)$  can be used for MI evaluation instead of the unknown real transition probability  $P_{Y|X}(y|x)$ . Thus, the lower bound of the MI can be derived as

$$\begin{aligned}
 I(X; Y) \geq R_{SYM} = & - \sum_{x' \in \chi} P_X(x') \log_2 P_X(x') \\
 & + \sum_{x' \in \chi} P_X(x') \int_C Q_{Y|X}(y|x') \\
 & \times \log_2 \frac{Q_{Y|X}(y|x') P_X(x')}{\sum_{x' \in \chi} Q_{Y|X}(y|x') P_X(x')} dy \quad (4)
 \end{aligned}$$

where  $R_{SYM}$  is the information rate that can be achieved by soft-decision FEC coding. In an AWGN auxiliary channel, we have

$$Q_{Y|X}(y|x) = \frac{1}{\sqrt{\pi}\sigma} \exp\left(\frac{-|y-x|^2}{\sigma^2}\right) \quad (5)$$

where  $\sigma^2$  is the noise variance for QAM formats.  $R_{SYM}$  can be calculated by integration, or approximated by the Monte

Carlo integration. In the Monte Carlo integration, a series of symbols, denoted by  $X^n = X_1, X_2, \dots, X_n$ , are selected from  $\mathcal{Y}$  following the probability distribution  $P_X(x)$ , sent through the AWGN auxiliary channel, and received as  $Y^n = Y_1, Y_2, \dots, Y_n$ . The lower bound MI can be estimated as [35]

$$\begin{aligned}
 R_{SYM} \approx & - \sum_{x' \in \chi} P_X(x') \log_2 P_X(x') \\
 & + \frac{1}{n} \sum_{i=1}^n Q_{X|Y}(x|Y_i) \log_2 Q_{X|Y}(x|Y_i) \quad (6)
 \end{aligned}$$

where  $Q_{X|Y}(x|Y_i)$  is the conditional probability that a specific  $x$  is sent when the sample  $Y_i$  is received,

$$\begin{aligned}
 Q_{X|Y}(x|Y_i) = & \frac{Q_{Y|X}(Y_i|x) P_X(x)}{Q_Y(Y_i)} \\
 = & \frac{\exp\left(\frac{-|Y_i-x|^2}{\sigma^2}\right) P_X(x)}{\sum_{x' \in \chi} \exp\left(\frac{-|Y_i-x'|^2}{\sigma^2}\right) P_X(x')} \quad (7)
 \end{aligned}$$

The estimated  $R_{SYM}$  from (6) and (7) closely approach the lower bound MI, when  $n$  is large enough. Specifically, in regular MQAM or GS-MQAM based communication systems,

$P_X(x) = 1/M$ , and we have that

$$R_{SYM} \approx \log_2 M + \frac{1}{n} \sum_{i=1}^n \frac{\exp(-|Y_i-x|^2/\sigma^2)}{\sum_{x' \in \mathcal{X}} \exp(-|Y_i-x'|^2/\sigma^2)} \log_2 \frac{\exp(-|Y_i-x|^2/\sigma^2)}{\sum_{x' \in \mathcal{X}} \exp(-|Y_i-x'|^2/\sigma^2)} \quad (8)$$

**C. MI COMPARISONS BETWEEN REGULAR, PS- AND GS-MQAM**

Given that MI is measured assuming the ideal FEC coding, we can generalize (2) to obtain PS-8/16/32QAM distributions in the complex 2D space, by replacing the real  $x$  in (2) as the complex amplitude. Please notice that star-8QAM is selected as the regular 8QAM and probabilistically shaped according to (2). The constellations of PS-8/16/32QAM with entropy loss of 0.25 bits/symbol (b/s) are illustrated in Figs. 3 (a2)-(c2), respectively. To simplify the description for the PS-MQAM with an entropy of  $E$  b/s, the following notation PS-MQAME is used, e.g., PS-16QAM3.5. We compare the MI performances of the shaped QAM formats with different entropies, in order to show the best shaping scheme for a given signal constellation size. Figure 4 shows the MI performances obtained by Monte Carlo integration. The entropies of PS-MQAM are selected from the range of  $[(\log_2 M) - 0.5, \log_2 M]$ . Clearly, GS-8QAM and GS-16QAM always reach the best performance, as shown Figs. 4 (a) and (b). PS-8/16QAM formats fail to achieve shaping gain in the regions of high SNR. While PS-8QAM2.875, PS-8QAM2.75, and PS-8QAM2.625 are able to outperform regular 8QAM when the SNRs are less than 9.4 dB, 7.8 dB, and 6.3 dB, respectively. By comparing the GS-16QAM with the PS-16QAM formats, we observe that their performances are quite similar when the SNR regions are upper-bounded by 11.5 dB, 10.1 dB, and 9.5 dB for PS-16QAM3.875, PS-16QAM3.75, and PS-16QAM3.625, respectively. But the best MI performance, as shown in Fig. 4 (c), cannot be acquired by any single 32QAM format. What is clear is that the performance of regular 32QAM is always worse than that of GS-32QAM. In the SNR region of 13.2-15.7dB, PS-32QAM4.875 offers the best performance. The performance of GS-32QAM is comparable to that PS-32QAM4.875 when the SNR is less than 13.2 dB, and reaches the largest shaping gain when the SNR is more than 15.7dB. In addition, GS-32QAM outperforms PS-32QAM4.75 and PS-32QAM4.625, respectively, in the SNR region lower-bounded by 13.9 and 13.3 dB. If 8-ary or/and 16-ary constellations are required for a transmission system, it is preferred to use GS scheme. In case of 32-ary constellation, the best solution depends on the realistic channel SNR region. We briefly summarize the analysis above, and list in TABLE 1 the optimal shaping schemes and the corresponding shaping gains in specific SNR regions.

If only PS scheme can be applied in a certain transmission system, it is also useful to compare the MI performances of

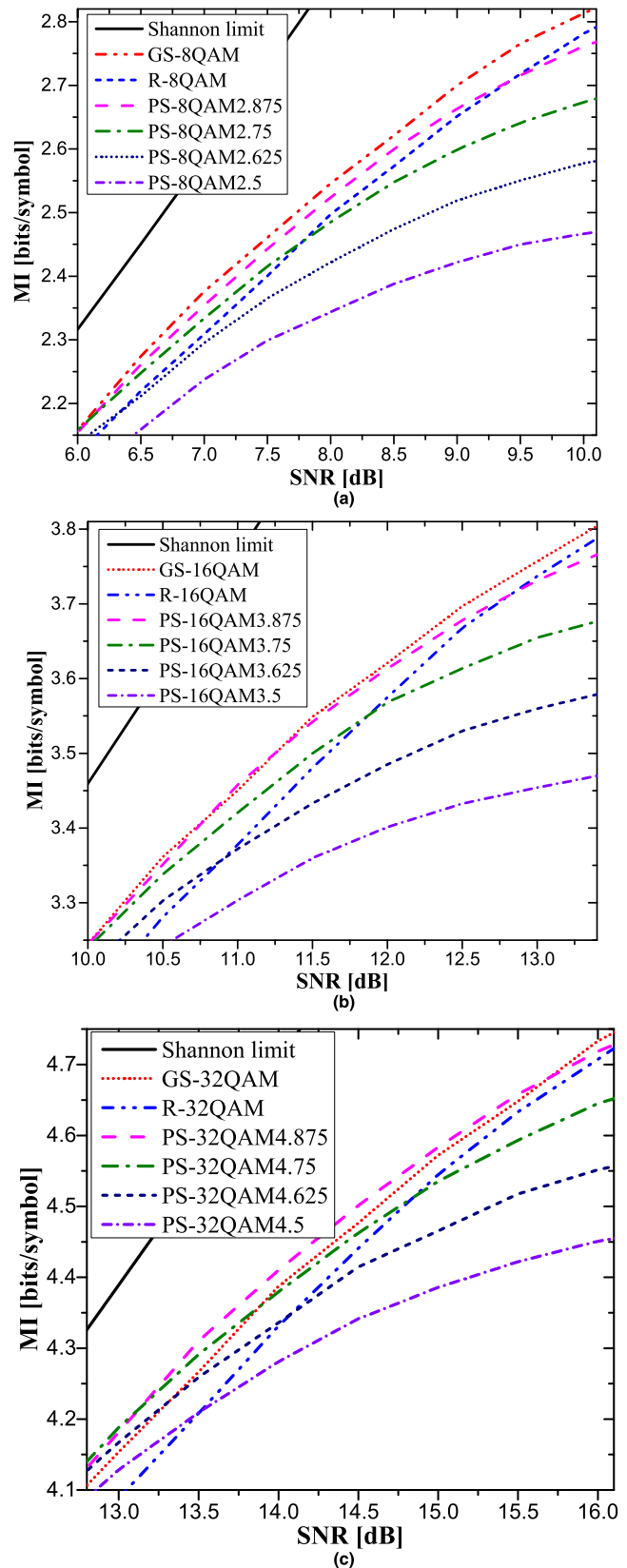


**FIGURE 4.** MI performances estimated from AWGN channels as a function of the SNR for (a) 8QAM, (b) 16QAM, (c) 32QAM. R-QAM: regular QAM.

PS-8/16/32QAM under the condition of the same entropy. Here, we use entropies of 2.7 b/s and 3.7 b/s as references. Figure 5 shows the MI performances of PS-8/16/32QAM

TABLE 1. Optimal Shaping Schemes in AWGN Channels.

MQAM	SNR [dB]	PS	GS	Shaping gain over R-MQAM
8QAM	<6	✓	✓	0.3 dB @ MI=2.5 b/s
	>6	✗	✓	0.2 dB @ MI=2.1 b/s
16QAM	<11.5	✓	✓	0.4 dB @ MI=3.5 b/s
	>11.5	✗	✓	0.2 dB @ MI=3.7 b/s
32QAM	<15.7	✓	✗	0.5 dB @ MI=4.1 b/s
	>15.7	✗	✓	0.2 dB @ MI=4.7 b/s

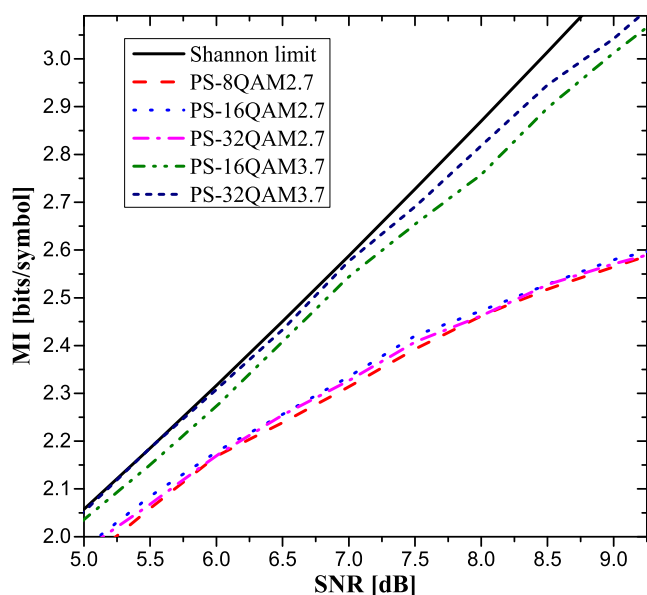


FIGURE 5. MI performances estimated from AWGN channels as a function of the SNR for PS-8/16/32QAM, when the entropy is fixed.

with the entropy of 2.7 b/s, as well as the MI performances of PS-16/32QAM with the entropy of 3.7 b/s. When the entropy is 2.7 b/s, the MI performance of PS-8QAM is slightly worse than that of the PS-16/32QAM, and there is no distinct difference between the MI performances of PS-16QAM and PS-32QAM. Considering the potential implementation penalty and DSP penalty in a realistic experimental setup, it is suggested to use PS-8QAM2.7 scheme or PS-16QAM2.7 scheme. When the entropy is 3.7 b/s, the MI performance of PS-32QAM is better than PS-16QAM. It is because PS-32QAM can achieve a more Gaussian-like distribution.

### III. EXPERIMENTAL DEMONSTRATION

#### A. EXPERIMENTAL SETUP

The diagram of the hardware based experimental setup is depicted in Fig. 6. Given that 8QAM based transmission channel only carries less than 3b/s, and 32QAM constellation will introduce much unknown implementation penalty,

we select 16QAM formats for the experimental comparison. At the transmitter side, the continuous wave (CW) light beam with the wavelength centered at 1550 nm is generated from a laser with a linewidth smaller than 10 kHz, and sent to a PM-I/Q modulator. The binary data sequence is uniformly mapped to 16QAM constellation for regular 16QAM signal generation; non-uniformly mapped to PS-16QAM3.75 and PS-16QAM3.5 symbols by DM; or mapped to GS-16QAM symbols with equal probability. Then the symbols are pulse shaped with the help of an arbitrary waveform generator (AWG) to generate 12.5G Baud PM-regular/PS/GS-16QAM signals. After being amplified by a booster erbium-doped fiber amplifier (EDFA), the signals are launched into a 100-km fiber link with the launch power of about -7 dBm. At the receiver side, the ASE noise-loading stage is constructed by two EDFAs cascaded with a variable optical attenuator (VOA). Two EDFAs are used in such ASE noise-loading stage to achieve a better OSNR resolution.

At the receiver side, the optical signal is pre-amplified by a EDFA and filtered by a optical tubule filter (OTF). Another laser with a linewidth less than 10 kHz serves as a local oscillator (LO) laser. The received signals are mixed with the LO light beam in the integrated coherent receiver (ICR), and digitalized by a real-time oscilloscope with 100 GSa/s sample rate and 33 GHz analog bandwidth. The captured signals are equalized and recovered by off-line DSP algorithms, including chromatic dispersion compensation, resampling, channel equalization using constant modulus algorithm (CMA) [1], and carrier phase recovery [36]. In order to minimize the DSP penalty, all the 16QAM signals are processed with a 5% pilot-assisted multi-modulus algorithm (MMA) after the pre-convergence by CMA. The MI performances are analyzed after the phase recovery. The recovered constellation diagrams for PM-16QAM, PM-GS-16QAM3.75, and PM-PS-16QAM3.5 are illustrated in insets (a-d) of Fig. 4, respectively. Notice that the entropy values of 3.5 and 3.75 are chosen to represent the deep shaping and shallow shaping cases respectively.

#### B. EXPERIMENTAL RESULTS AND ANALYSIS

The experimentally obtained MI performances as a function of OSNR are summarized in Fig. 7. Notice that the MI values shown in Fig. 7 are measured without the consideration of channel coding. A soft-decision low-density parity-check (LDPC) coding with a BER threshold of less than 0.07 is suggested to obtain robust and error-free post-FEC performance. Because featured with a non-uniform constellation diagram, GS-16QAM, compared to regular 16QAM, are more sensitive to DSP penalty and implementation penalty. In our experiment, the implementation penalty and DSP penalty exceed 2.5 dB in total. As a result, the MI performance of GS-16QAM is inferior to that of the PS-16QAM formats, when the OSNR is smaller than 9.5 dB. While the GS-16QAM, over a wide range of OSNR values, can still obtain the best MI performance. More precisely, GS-16QAM can always outperform regular 16QAM; when the OSNR is larger than 10.2 dB,

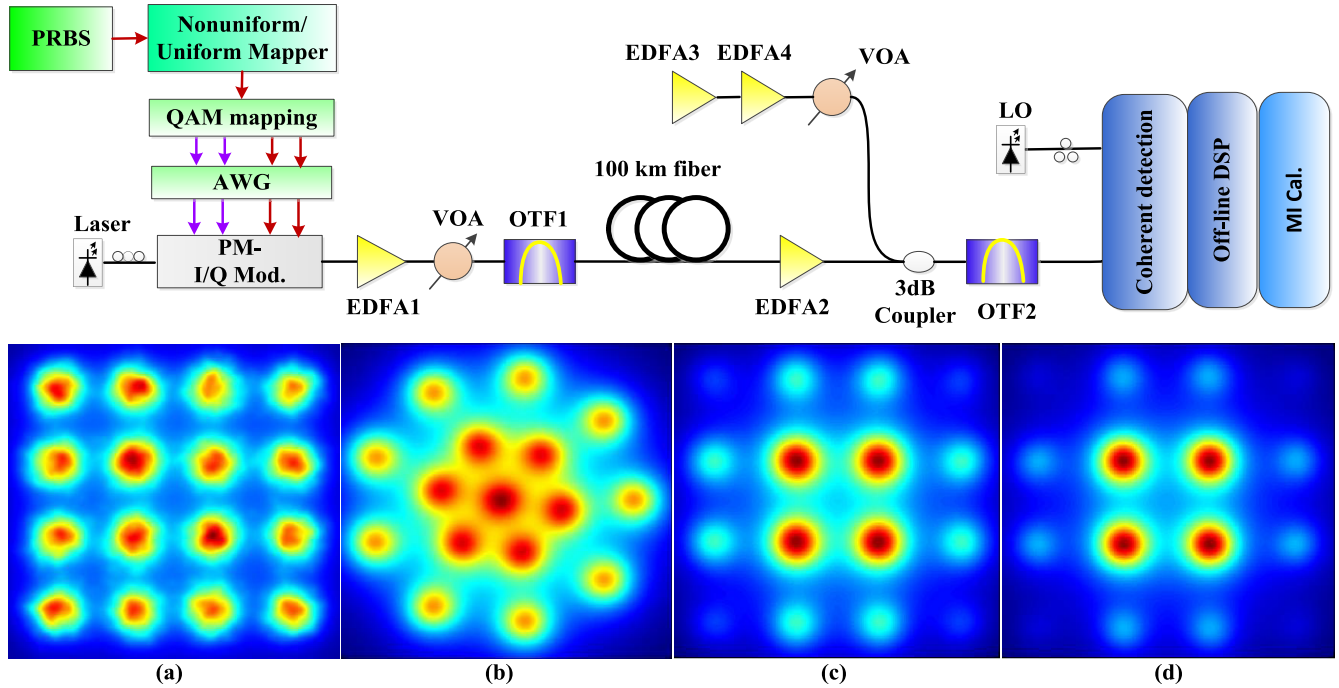


FIGURE 6. Experimental setup. Insets: the recovered constellation diagrams for (a) regular PM-16QAM, (b) PM-GS-16QAM, (c) PM-PS-16QAM 3.75, (d) PM-PS-16QAM 3.5.

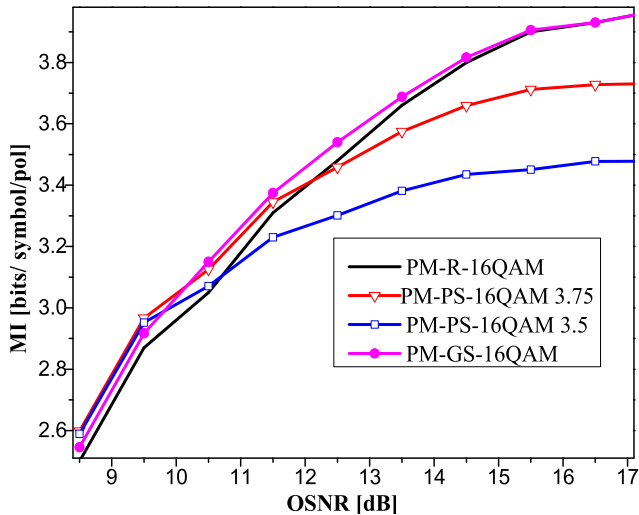


FIGURE 7. Experimentally obtained MI performances as a function of the OSNR for PM-16QAM formats.

and an increasing shaping gain over PS-16QAM3.75 can be experimentally obtained. Compared to PS-16QAM3.5, GS-16QAM is able to carry more bits/symbol when the OSNR is larger than 9.7 dB. The advantage of GS-16QAM over PS-16QAM can be attributed to the fact that in a 16-ary 2D constellation, GS is able to lay-out the 16 points towards a more Gaussian-like distribution.

#### IV. NONLINEAR TOLERANCE

##### A. EGN MODEL AND NONLINEAR NOISE

In a fiber-optic transmission system, the channel link is affected by the linear ASE noise and nonlinear interference

noise (NLIN). The variance of channel noise is given by

$$\sigma^2 = \sigma_{ASE}^2 + \sigma_{NLIN}^2 \tag{9}$$

where  $\sigma_{ASE}^2$  and  $\sigma_{NLIN}^2$  denote the variances of ASE noise and NLIN, respectively. In a classical GN model [34], NLIN is described as an additive Gaussian noise, which is modulation independent. In contrast, the recently proposed EGN model provides a more accurate prediction in multi-span transmission systems, since the effect of modulation on NLIN has been taken into account [37]. In our simulation platform, the accumulation of NLIN is obtained by the EGN model, and the accumulated ASE noise is added to the optical signals after each span. Assuming the channel distortion has been well compensated, the channel noise can be measured as

$$SNR_{eff} = \frac{P}{\sigma_{ASE}^2 + \chi P^3} = \frac{P}{\sigma_{ASE}^2 + [\chi_0 + \chi_4(\mu_4 - 2) + (\mu_4 - 2)^2 \chi_4' + \mu_6 \chi_6] P^3} \tag{10}$$

where  $P$  is the average launch power,  $\chi$ ,  $\chi_0$ ,  $\chi_4$ ,  $\chi_4'$ , and  $\chi_6$  are the real coefficients indicating the contributions of fiber nonlinearities,  $\mu_4$  and  $\mu_6$  are the standardized 4<sup>th</sup> and 6<sup>th</sup> moments of the channel input  $X$ , which are defined as

$$\mu_k = \frac{\mathbb{E}[|X - \mathbb{E}(X)|^k]}{\mathbb{E}[|X - \mathbb{E}(X)|^2]^{k/2}} \tag{11}$$

where  $\mathbb{E}[\cdot]$  denotes expectation operation. By setting the derivative of (10) to 0, the optimal launch power for a specific

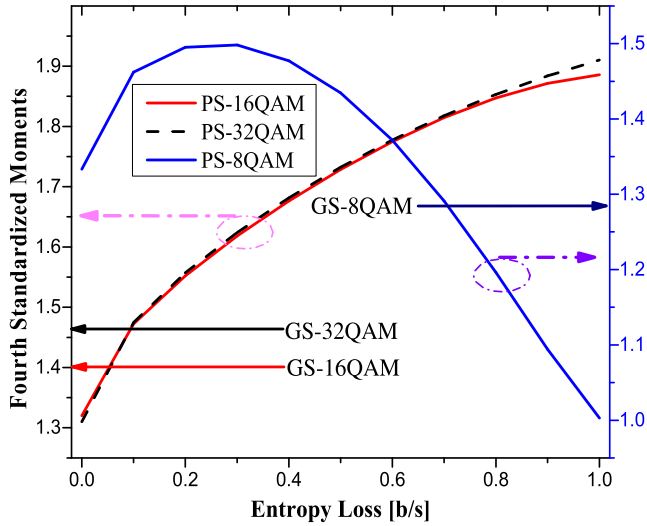


FIGURE 8. Measured  $\mu_4$  values as a function of the entropy loss for PS-8/16/32QAM formats.

transmission distance is given as

$$P_{\text{opt}} = \left( \frac{\sigma_{\text{ASE}}^2}{2\chi} \right)^{1/3} \quad (12)$$

Considering  $\chi'_4$  and  $\chi_6$  are far less than  $\chi_4$ , we investigate only the  $\mu_4$  values for regular/PS/GS-MQAM. The higher  $\mu_4$  is, the stronger modulation-dependent NLIN will be suffered by a given QAM format. Figure 8 summarizes the measured  $\mu_4$  values for PS-8/16/32QAM formats, as well as the GS-8/16/32QAM formats. The entropy loss region for each PS-MQAM format is selected from 0b/s (corresponding to regular MQAM) to 1b/s (corresponding to PS-MQAM with entropy of  $\log_2 M - 1$ ). We find that the  $\mu_4$  values carried by PS-16QAM and PS-32QAM are quite similar;  $\mu_4$  is not a monotonically increasing function for deeper shaped 8QAM, and PS-8QAM2.75 features the maximum  $\mu_4$ . Meanwhile, the  $\mu_4$  values are measured as 1.28, 1.4, and 1.46 for GS-8QAM, GS-16QAM, and GS-32QAM, respectively, corresponding to PS-8QAM2.3, PS-16QAM3.95, and PS-32QAM4.9, respectively. Interestingly, GS-8QAM has a smaller  $\mu_4$  value than regular 8QAM. Generally speaking, GS-MQAM formats suffer less modulation-dependent NLIN than PS-MQAM. We think it is because that in the GS-8QAM constellation, there are 6 points located in the outer power layer and 2 points in the inner layer, which is more like one-modulus constellation; in the GS-16/32QAM constellations, the null-power point located in the central position will not contribute the modulation-dependent NLIN.

**B. REACH INCREASE BY SHAPING TECHNIQUE**

The channel parameters used in the EGN model are summarized in Table 2. Notice that the MI values are not calculated with nonlinear noise compensation, but with the launch power optimized for each span according to (12).

TABLE 2. System Parameters Used in The Simulation.

Parameter	Specification
Modulation format	R/PS/GS-MQAM
Symbol rate	32 GHz
Polarization	Dual-polarization
Fiber type	SSMF
WDM channels	15
WDM spacing	50 GHz
Span length	100 km
Attenuation	0.2 dB/km
Dispersion	17 ps/nm/km
Nonlinear coefficient	1.3 W/km
Amplifier	EDFA
EDFA noise figure	5 dB

Figure 9 shows the numerically measured MI performances as a function of transmission distance for 8/16/32QAM formats. As shown in Fig. 9 (a), GS-8QAM offers the best performance along the long-distance transmission; while regular 8QAM fails to provide a larger MI than PS-8QAM2.875 and PS-8QAM2.75 after 55 and 78 spans, respectively. When the MI is 2.5 b/s, GS-8QAM provides 500 km and 700 km reach improvement over PS-8QAM2.875 and regular 8QAM, respectively. Such great reach improvements fully reveal that GS-8QAM is a power-efficient and NLIN tolerant 8-ary modulation format. In Fig. 9 (b), GS-16QAM has the best performance during the multi-span transmission; regular 16QAM and PS-16QAM3.875 offer comparable performances against GS-16QAM before 25 spans, and after 37 spans, respectively. Further, PS-16QAM3.875, PS-16QAM3.75, PS-16QAM3.625, and PS-16QAM3.5 start to outperform regular 16QAM after 26, 28, 43, and 53 spans, respectively. GS-16QAM and PS-16QAM3.875 can extend the reach over regular 16QAM by 7.7%, at the MI of 3.2 b/s. In Fig. 9 (c), the performance of regular 32QAM is slightly better than that of GS-32QAM when the transmission distance is up to 13 spans, because regular 32QAM suffer the least modulation-dependent NLIN; while GS-32QAM can outperform regular 32QAM after 20 spans, because GS-32QAM has a better tolerance against the accumulated ASE noise. Within the transmission range from 15 spans to 28 spans, PS-32QAM3.875 clearly has the best performance, but PS-32QAM3.75 shows better performance after that. In addition, PS-32QAM4.75, PS-32QAM4.625, and PS-32QAM4.5 show better performances against regular 32QAM after 19 spans, 22 spans, and 25 spans, respectively. In case of MI=4 b/s, PS-32QAM4.875 and GS-32QAM are able to obtain reach increase over regular 32QAM by 7% and 4.3%, respectively. In the presence of NLIN, a desirable GS-QAM format should be optimized with (9) taken into account. Therefore, the best GS-MQAM formats depend on the transmission distance.

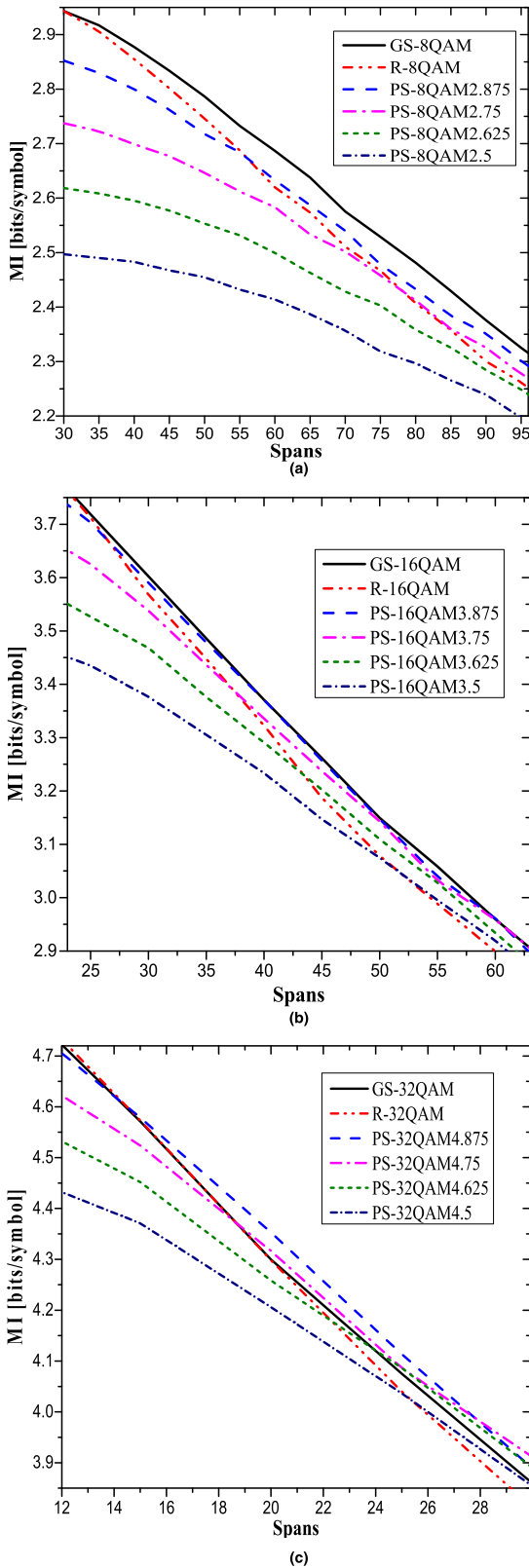


FIGURE 9. MI performances as a function of transmission distance for: (a) 8QAM. (b) 16QAM, and (c) 32QAM.

To facilitate the readers' understanding, we list in TABLE 3 the optimal shaping schemes and corresponding reach improvement in specific distance ranges.

TABLE 3. Optimal Shaping Schemes in Multi-span Transmission Systems.

MQAM	Spans	PS	GS	Reach improvement over R-MQAM
8QAM	Whole	×	✓	10% @ MI=2.5 b/s
16QAM	<37	×	✓	5% @ MI=3.5 b/s
	>37	✓	✓	7.7% @ MI=3.2 b/s
32QAM	<13	×	×	N/A
	>13	✓	×	7% @ MI=4 b/s

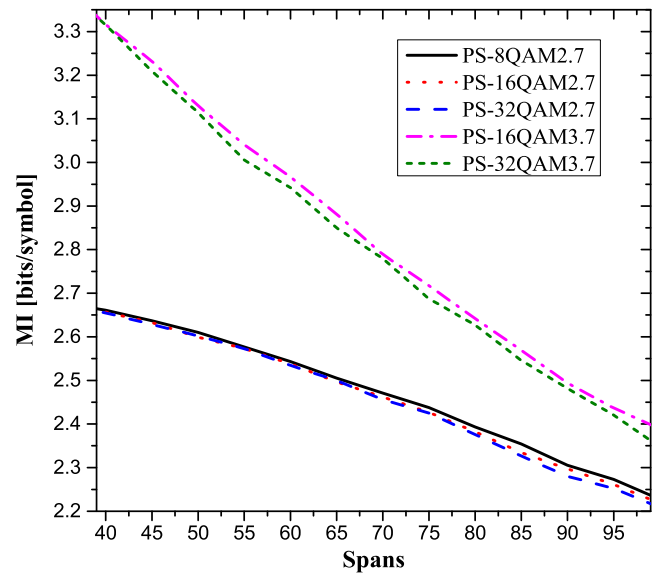


FIGURE 10. MI performances as a function of transmission distance for PS-8/16/32QAM, when the entropy is fixed.

If only PS scheme can be used, it is necessary to compare the MI performances of PS-8/16/32QAM as a function of transmission distance. Figure 10 shows the MI performances of PS-8/16/32QAM with the entropy of 2.7 b/s, and the MI performances of PS-16/32QAM with the entropy of 3.7 b/s. When the entropy is 2.7 b/s, the  $\mu_4$  values of PS-8QAM, PS-16QAM, and PS-32QAM are measured as 1.49, 1.85, and 1.89, respectively. Accordingly, PS-8QAM has a better MI performance than PS-16/32QAM after 65 spans. When the entropy is 3.7 b/s, the  $\mu_4$  values of PS-16QAM and PS-32QAM are measured as 1.62 and 1.97, respectively. When the transmission distance is longer than 42 spans, PS-16QAM offers a better solution than PS-32QAM.

In a long-haul transmission system, it is worthwhile to notice that the accumulated NILN and ASE noise may not yield a Gaussian distribution. As a result, the optimal PS-MQAM scheme is supposed not to follow the M-B distribution. Similarly, the optimal GS-MQAM formats should also be different from the ones obtained from Gaussian noise. There is no theoretical analysis so far to easily achieve the best PS or GS schemes. Greedy-searching needs to be

performed to find the optimal PS-MQAM distribution; while our proposed 6-steps GS-MQAM generation procedure is required to be re-run according to the real noise distribution at a specific distance. Finally, the summation of the obtained PS/GS-MQAM signal distribution and the specific noise distribution should again approach a Gaussian distribution.

## V. CONCLUSION

We have introduced a GS-MQAM generation procedure, which minimizes the mean-square error of optimum source representation. Regular 8/16/32QAM formats, GS-8/16/32QAM formats, and PS-8/16/32QAM formats have been compared in terms of MI performance. In an ASE-noise dominated channel, GS-8/16QAM could offer the best performance; while PS-32QAM and GS-32QAM provided the largest shaping gains separately in certain SNR regions. We also investigated the nonlinear noise tolerance for 8/16/32QAM formats, and found that GS-8/16/32QAM generally suffer lower modulation-dependent NLIN than PS-8/16/32QAM. GS-8/16QAM could extend the reach in the EGN model based multi-span transmission system. In addition, PS-32QAM formats showed better performance over a relatively long transmission distance. A GS-QAM scheme optimized in the presence of NLIN and ASE noise is suggested for a multi-span transmission system.

Although in principle offers a great performance, PS-64QAM inevitably suffers implementation penalty and DSP penalty in a realistic experiment, because of the large constellation size of 64QAM. Shaped 8/16/32QAM can still be expected to play important roles in the future optical transport networks. An implementation-friendly shaping scheme will attract more attentions in the future, as well as the hybrid probabilistic-geometric shaping schemes to optimize the GMI performance.

## REFERENCES

- [1] S. J. Savory, "Digital coherent optical receivers: Algorithms and sub-systems," *IEEE J. Sel. Topics Quantum Electron.*, vol. 16, no. 5, pp. 1164–1179, Sep./Oct. 2010.
- [2] Z. Qu, S. Fu, M. Zhang, M. Tang, P. Shum, and D. Liu, "Analytical investigation on self-homodyne coherent system based on few-mode fiber," *IEEE Photon. Technol. Lett.*, vol. 26, no. 1, pp. 74–77, Jan. 1, 2014.
- [3] J. Zhang *et al.*, "Simplified coherent receiver with heterodyne detection of eight-channel 50 Gb/s PDM-QPSK WDM signal after 1040 km SMF-28 transmission," *Opt. Lett.*, vol. 37, no. 19, pp. 4050–4052, Oct. 2012.
- [4] X. Zhou *et al.*, "64-Tb/s, 8 b/s/Hz, PDM-36QAM transmission over 320 km using both Pre- and post-transmission digital signal processing," *J. Lightw. Technol.*, vol. 29, no. 4, pp. 571–577, Feb. 15, 2011.
- [5] M. Nakazawa, S. Okamoto, T. Omiya, K. Kasai, and M. Yoshida, "256-QAM (64 Gb/s) coherent optical transmission over 160 km with an optical bandwidth of 5.4 GHz," *IEEE Photon. Technol. Lett.*, vol. 22, no. 3, pp. 185–187, Feb. 1, 2010.
- [6] J. Sakaguchi *et al.*, "Space division multiplexed transmission of 109-Tb/s data signals using homogeneous seven-core fiber," *J. Lightw. Technol.*, vol. 30, no. 4, pp. 658–665, Feb. 15, 2012.
- [7] P. Sillard, M. Bigot-Astruc, and D. Molin, "Few-mode fibers for mode-division-multiplexed systems," *J. Lightw. Technol.*, vol. 32, no. 16, pp. 2824–2829, Aug. 15, 2014.
- [8] Z. Qu *et al.*, "Performance optimization of PM-16QAM transmission system enabled by real-time self-adaptive coding," *Opt. Lett.*, vol. 42, no. 20, pp. 4211–4214, Oct. 2017.
- [9] G. Forney, R. Gallager, G. Lang, F. Longstaff, and S. Qureshi, "Efficient modulation for band-limited channels," *IEEE J. Sel. Areas Commun.*, vol. JSAC-2, no. 5, pp. 632–647, Sep. 1984.
- [10] F. R. Kschischang and S. Pasupathy, "Optimal nonuniform signaling for Gaussian channels," *IEEE Trans. Inf. Theory*, vol. 39, no. 3, pp. 913–929, May 1993.
- [11] E. Pisek, D. Rajan, S. Abu-Surra, and J. R. Cleveland, "Capacity-approaching TQC-LDPC convolutional codes enabling power-efficient decoders," *IEEE Trans. Commun.*, vol. 65, no. 1, pp. 1–13, Jan. 2017.
- [12] G. D. Forney and L.-F. Wei, "Multidimensional constellations. I. Introduction, figures of merit, and generalized cross constellations," *IEEE J. Sel. Areas Commun.*, vol. 7, no. 6, pp. 877–892, Aug. 1989.
- [13] G. D. Forney, "Multidimensional constellations. II. Voronoi constellations," *IEEE J. Sel. Areas Commun.*, vol. 7, no. 6, pp. 941–958, Aug. 1989.
- [14] A. R. Calderbank and L. H. Ozarow, "Nonequiprobable signaling on the Gaussian channel," *IEEE Trans. Inf. Theory*, vol. 36, no. 4, pp. 726–740, Jul. 1990.
- [15] R. G. Gallager, *Information Theory and Reliable Communication*. Hoboken, NJ, USA: Wiley, 1968.
- [16] Z. Qu, C. Lin, T. Liu, and I. B. Djordjevic, "Experimental investigation of GF(3<sup>2</sup>) nonbinary LDPC-coded non-uniform 9-QAM modulation format," in *Proc. 42nd Eur. Conf. Opt. Commun. (ECOC)*, Sep. 2016, pp. 1–3.
- [17] Z. Qu, C. Lin, T. Liu, and I. B. Djordjevic, "Experimental study of non-linearity tolerant modulation formats based on LDPC coded non-uniform signaling," in *Proc. Opt. Fiber Commun. Conf. Exhib. (OFC)*, Mar. 2017, pp. 1–3, Paper W1G.7.
- [18] J.-X. Cai *et al.*, "70.4 Tb/s capacity over 7,600 km in C+L band using coded modulation with hybrid constellation shaping and nonlinearity compensation," in *Proc. Opt. Fiber Commun. Conf. Exhib. (OFC)*, Mar. 2017, pp. 1–3, Paper Th5B.2.
- [19] H. G. Batshon, I. B. Djordjevic, L. Xu, and T. Wang, "Iterative polar quantization-based modulation to achieve channel capacity in ultrahigh-speed optical communication systems," *IEEE Photon. J.*, vol. 2, no. 4, pp. 593–599, Aug. 2010.
- [20] S. Zhang, F. Yaman, E. Mateo, T. Inoue, K. Nakamura, and Y. Inada, "A generalized pairwise optimization for designing multi-dimensional modulation formats," in *Proc. Opt. Fiber Commun. Conf. Exhib. (OFC)*, Mar. 2017, pp. 1–3, Paper W4A.6.
- [21] J. Karout, R.-J. Essiambre, E. Agrell, and A. Tulino, "Achievable rates of multidimensional multisphere distributions," in *Proc. Opt. Fiber Commun. Conf. Exhib. (OFC)*, Mar. 2017, pp. 1–4, Paper W4A.4.
- [22] G. D. Forney, "Trellis shaping," *IEEE Trans. Inf. Theory*, vol. 38, no. 2, pp. 281–300, Mar. 1992.
- [23] A. K. Khandani and P. Kabal, "Shaping multidimensional signal spaces. I. Optimum shaping, shell mapping," *IEEE Trans. Inf. Theory*, vol. 39, no. 6, pp. 1799–1808, Nov. 1993.
- [24] P. Schulte and G. Böcherer, "Constant composition distribution matching," *IEEE Trans. Inf. Theory*, vol. 62, no. 1, pp. 430–434, Jan. 2016.
- [25] G. Böcherer, P. Schulte, and F. Steiner, "Bandwidth efficient and rate-matched low-density parity-check coded modulation," *IEEE Trans. Commun.*, vol. 63, no. 12, pp. 4651–4665, Dec. 2015.
- [26] F. Steiner and G. Böcherer, "Comparison of geometric and probabilistic shaping with application to ATSC 3.0," in *Proc. 11th Int. ITG Conf. Syst. Commun. Coding (SCC)*, Hamburg, Germany, Feb. 2017, pp. 1–6.
- [27] J. Cho *et al.*, "Trans-Atlantic field trial using probabilistically shaped 64-QAM at high spectral efficiencies and single-carrier real-time 250-Gb/s 16-QAM," in *Proc. Opt. Fiber Commun. Conf. Exhib. (OFC)*, Mar. 2017, pp. 1–3, Paper Th5B.3.
- [28] T. Fehenberger, A. Alvarado, G. Böcherer, and N. Hanik, "On probabilistic shaping of quadrature amplitude modulation for the nonlinear fiber channel," *J. Lightw. Technol.*, vol. 34, no. 21, pp. 5063–5073, Nov. 1, 2016.
- [29] T. Liu and I. B. Djordjevic, "Multidimensional optimal signal constellation sets and symbol mappings for block-interleaved coded-modulation enabling ultrahigh-speed optical transport," *IEEE Photon. J.*, vol. 6, no. 4, Aug. 2014, Art. no. 5500714.
- [30] Z. Qu and I. B. Djordjevic, "Geometrically shaped 16QAM outperforming probabilistically shaped 16QAM," in *Proc. Eur. Conf. Opt. Commun. (ECOC)*, Sep. 2017, pp. 1–3, Paper Th.2.F.4.
- [31] A. Leven, F. Vacondio, L. Schmalen, S. ten Brink, and W. Idler, "Estimation of soft FEC performance in optical transmission experiments," *IEEE Photon. Technol. Lett.*, vol. 23, no. 20, pp. 1547–1549, Oct. 15, 2011.

- [32] A. Alvarado, E. Agrell, D. Lavery, R. Maher, and P. Bayvel, "Replacing the soft-decision FEC limit paradigm in the design of optical communication systems," *J. Lightw. Technol.*, vol. 33, no. 20, pp. 4338–4352, Oct. 15, 2015.
- [33] D. M. Arnold, H.-A. Loeliger, P. O. Vontobel, A. Kavcic, and W. Zeng, "Simulation-based computation of information rates for channels with memory," *IEEE Trans. Inf. Theory*, vol. 52, no. 8, pp. 3498–3508, Aug. 2006.
- [34] T. Fehenberger, A. Alvarado, P. Bayvel, and N. Hanik, "On achievable rates for long-haul fiber-optic communications," *Opt. Express*, vol. 23, no. 7, pp. 9183–9191, Apr. 2015.
- [35] A. Carena, V. Curri, G. Bosco, P. Poggiolini, and F. Forghieri, "Modeling of the impact of nonlinear propagation effects in uncompensated optical coherent transmission links," *J. Lightw. Technol.*, vol. 30, no. 10, pp. 1524–1539, May 15, 2012.
- [36] T. Pfau, S. Hoffmann, and R. Noe, "Hardware-efficient coherent digital receiver concept with feedforward carrier recovery for  $M$ -QAM constellations," *J. Lightw. Technol.*, vol. 27, no. 8, pp. 989–999, Apr. 15, 2009.
- [37] P. Poggiolini, G. Bosco, A. Carena, V. Curri, Y. Jiang, and F. Forghieri, "The GN-model of fiber non-linear propagation and its applications," *J. Lightw. Technol.*, vol. 32, no. 4, pp. 694–721, Feb. 15, 2014.



tions in the last two years. He is a Student Member of OSA and IEEE.

**ZHEN QU** was born in Shandong, China. He received the Diploma degree from the College of Physics, University of Jinan, and the master's degree from the College of Optical and Electrical Information, Huazhong University of Science and Technology. He is currently pursuing the Ph.D. degree with the Department of Electrical and Computer Engineering, The University of Arizona. He has authored or co-authored two book chapters and more than 30 journal and conference publica-



**IVAN B. DJORDJEVIC** is currently a Professor of electrical and computer engineering and optical sciences with The University of Arizona, the Director of the Optical Communications Systems Laboratory and Quantum Communications Lab, and the Co-Director of the Signal Processing and Coding Lab. Prior to joining the University of Arizona, he held appointments at the University of the West of England, University of Bristol, Tyco Telecommunications, National Technical University of Athens, Greece, and State Telecommunication Company, Yugoslavia. He has authored or co-authored six books, more than 460 journal and conference publications, and 43 U.S. patents.

Mr. Djordjevic is a Senior Member of the IEEE and a Fellow of OSA. He currently serves as an Editor and Associate Editor for the IEEE COMMUNICATIONS LETTERS and *Physical Communication* journal. He is also an Editorial Board Member for the *Journal of Optics* (IOP) and the (*Journal of RF-Engineering and Telecommunications*) (Frequenz).

...